A new analytical method for stability analysis of rock blocks with cavities in sub-horizontal strata by the considering eccentricity effect

Xushan Shi[1], Bo Chai[1,3,4], Juan Du[1,2,4], Wei Wang[1,3,4], Bo Liu[1]

[1]School of Environmental Studies, China University of Geosciences, Wuhan, 430078, China
[2]Centre for severe weather and climate and hydrogeological hazards, Wuhan, 430078, China
[3]Hubei Key Laboratory of Yangtze Catchment Environmental Aquatic Science, Wuhan, 430078, China
[4]Research Center for Geohazards Monitoring and Warning in Three Gorges Reservoir, Wanzhou, 404000, China

Correspondence to: Bo Chai (chaibo@cug.edu.cn) and Juan Du (dujuan@cug.edu.cn)

Abstract. The basal cavity of a rock block formed due to differential weathering is an important predisposing factor for rockfall in hard-soft interbedded rocks. Rock block falling due to the eccentricity effect with the failure modes of toppling or sliding is defined as biased rockfall in this study. Considering the non-uniform stress distribution due to the eccentricity effect, a new analytical method for three-dimensional stability analysis of biased rockfall is proposed. A set of factors of safety (Fos) against partial damage (compressive and tensile damage of the soft underlying layer) and overall failure (toppling and sliding of the hard rock block) are used to determine the rockfall susceptibility level. The analytical method is applied and validated with biased rockfalls on the northeast edge of the Sichuan Basin in Southwest China, where large amounts of rockfalls have developed, composed of overlying thick sandstone and underlying mudstone. The evolution process of biased rockfalls is divided into four stages, initial state, cavity formation, partial unstable and failure. The proposed method is validated by calculating Fos of the typical unstable rock blocks in the study area. The continuous retreat of cavity causes stress redistribution between the hard and soft rock layers. Consequently, the development of the eccentricity effect leads to damage to the underlying soft rock layer and further failure of the hard rock block. The critical cavity retreat ratio is determined to be 0.33 to classify the low and moderate rockfall susceptibility in the eastern Sichuan Basin. The proposed analytical method is effective for the early identification of biased rockfall, which is significant for rockfall prevention and risk mitigation.

List of symbols

|	
a	length of the block along the x direction
A	area of contact surfaces
b	width of the block along the y direction
c	cohesive force of the mudstone
d_i	width of the basal cavity in a certain direction
e_x	eccentric distance along the x direction
e_y	eccentric distance along the y direction

32	E_x	horizontal seismic force along the x direction
33	Fos	factor of safety
34	h	height of the block
35	h_w	height of the water in the fracture
36	H_x	water pressure along the x direction
37	I_x	moment of inertia with respect to the x-axis
38	I_y	moment of inertia with respect to the y-axis
39	k_e	earthquake contribution coefficient
40	k_1	rainfall coefficient, taking 1 in the rainfall scenario and 0 in the non-rainfall scenario
41	k_2	earthquake coefficient, taking 1 in the seismic scenario and 0 in the non-seismic scenario
42	k_3	free surface coefficient, taking 1 for two free surfaces and 0 for three free surfaces
43	M_{bx}	total bending moments with respect to the x-axis on the mudstone foundation
44	M_{by}	total bending moments with respect to the y-axis on the mudstone foundation
45	M_{bEx}	bending moment of E_x with respect to the x-axis on the mudstone foundation
46	M_{bHx}	bending moment of H_x with respect to the x-axis on the mudstone foundation
47	M_{bWx}	bending moment of W with respect to the x-axis on the mudstone foundation
48	M_{Ex}	overturning moment provided by E_x along the x direction
49	M_{Hx}	overturning moment provided by H_x along the x direction
50	M_{px}	stabilizing moment of p_n along the x direction
51	$M_{W_{inx}}$	stabilizing moment provided by W along the x direction
52	$M_{W_{outx}}$	overturning moment provided by W along the x direction
53	N_z	total applied vertical load on the mudstone base
54	O	origin of the (x, y) coordinates
55	$p(x, y)$	pressure magnitude at point (x, y)
56	r_i	the basal cavity retreat ratio equal to the ratio of cavity width to block width in a certain direction
57	W	weight of the block
58	x	distance to O along the x-axis
59	y	distance to O along the y-axis
60	α	true dip of the contact surface
61	γ_s	unit weight of sandstone
62	γ_w	unit weight of water
63	θ_1	apparent dip of α on plane J1
64	θ_2	apparent dip of α on plane J2

65	σ_{cmax}	ultimate compressive strength of the mudstone
66	σ_{tmax}	ultimate tensile strength of the mudstone
67	τ_{max}	ultimate shear strength of the mudstone
68	φ	friction angle of the mudstone
69	ω_1	angle between the trend of the contact surface and the x direction
70	ω_2	angle between the trend of the contact surface and the y direction

1 Introduction

Rockfall is defined as the detachment of a rock block from a steep slope along a surface, on which little or no shear displacement takes place (Cruden and Varnes, 1996). Rockfalls frequently occur in mountainous ranges, cut slopes, and coastal cliffs, and they may cause significant facility damage and casualties in residential areas and transport corridors (Chau et al., 2003; Volkwein et al., 2011; Corominas et al., 2018). Stability analysis of rock blocks are crucial for risk management and early warning of rockfall (Kromer et al., 2017).

Rockfall is widespread and poses high risk in the eastern Sichuan Basin, Southwest China (Chen et al., 2008; Chen and Tang, 2010; Zhang et al., 2016; Zhou et al., 2017; Zhou et al., 2018). The rockfall in this area is attributed to the tectonic setting of Jura-type folds and the stratum sequence, which is characterized by the interbedding of hard and soft layers. An alternation of thick sandstone and thin mudstone layers is formed in the wide and gentle-angle synclines (Zhang et al., 2015; Wu et al., 2018). Weathering is known to be one of the main predisposing factors for rockfall (Jaboyedoff et al., 2021; Zhan et al., 2022). The cliff comprised of hard sandstone is the source of rockfall, and the underlying mudstone is more susceptible to weathering. Along with the retreat of basal cavities in the mudstone layer, the gravity centre of the overlying sandstone block moves outward relative to the mudstone. In this case, the stress distribution in the contact surface of sandstone and mudstone is non-uniform. The mudstone on the outer side bears higher compressive stress than that on the inner side. This phenomenon can be defined as an eccentricity effect, which leads to mudstone damage and failure of the overlying sandstone by toppling or sliding. This type of rockfall is defined as biased rockfall in this study (Fig. 1). Similar rockfall patterns have been widely reported in other regions, such as Joss Bay in England (Hutchinson, 1972), Okinawa Island in Japan (Kogure et al., 2006), and the Colorado Plateau of the southwestern United States (Ward et al., 2011). Retreat of the basal cavity is a main cause for the failure of the overlying block. Therefore, it is necessary to establish an analytical method, considering the development of the basal cavity, to analyse the stress distribution and stability of rock blocks, which is fundamental to the susceptibility assessment and risk control of biased rockfall.
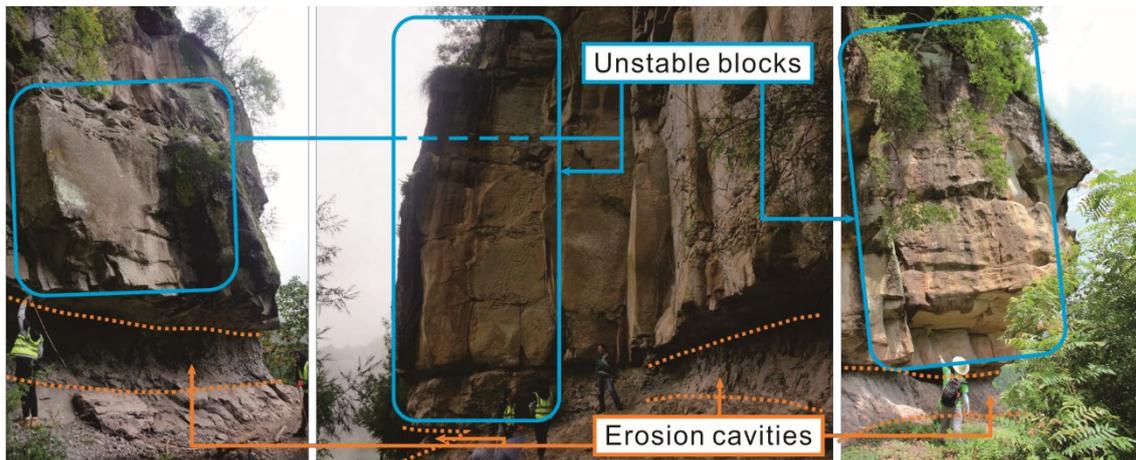
Figure 1 Potential unstable blocks and basal cavities caused by differential weathering.

Rockfall stability analysis methods include statistical analysis (Frattini et al., 2008; Santi et al., 2009), empirical rating systems (Pierson et al., 1990; Ferrari et al., 2016), and mechanical analysis (Jaboyedoff et al., 2004; Derron et al., 2005; Matasci et al., 2018). The statistical analysis and empirical rating systems are suitable for rockfall hazard assessment at a regional scale. The accuracy of statistical analysis depends on the completeness of rockfall inventories (Chau et al., 2003; Guzzetti et al., 2003; D'amato et al., 2016). However, its application to rockfall hazards is limited due to the lack of complete inventory data (Budetta and Nappi, 2013; Malamud et al., 2004). Empirical and semi-empirical rating systems are used where site-specific rockfall inventories are either unavailable or unreliable. Therefore, rockfall susceptibility can be assessed by heuristic ranking of selected predisposing factors (Frattini et al., 2008; Budetta, 2004). Mechanical analysis based on static equilibrium theory is the main method to analyse the stability of site-specific rockfall using the factor of safety (Fos). Ashby (1971) conducted stability analysis with a parallelepiped block resting on an inclined plane (Fig. 2a), and the solution was subsequently modified by Bray and Goodman (1981) and Sagaseta (1986). Kogure et al. (2006) utilized a cantilever beam model to determine the critical state of limestone cliffs. Frayssines and Hantz (2009) proposed the limit equilibrium method (LEM) to predict block stability against sliding and toppling in steep limestone cliffs (Fig. 2c). Chen and Tang (2010) established a stability analysis method of three types of unstable rocks in the Three Gorges Reservoir area with the LEM. Alejano et al. (2015) studied the influence of rounding of block corners on the block stability. Zhang et al. (2016) defined Fos based on fracture mechanics and studied the progressive failure process by analysing crack propagation. Alejano et al. (2010) and Pérez-Rey et al. (2021) deduced a formula for Fos of blocks with more complex geometry.
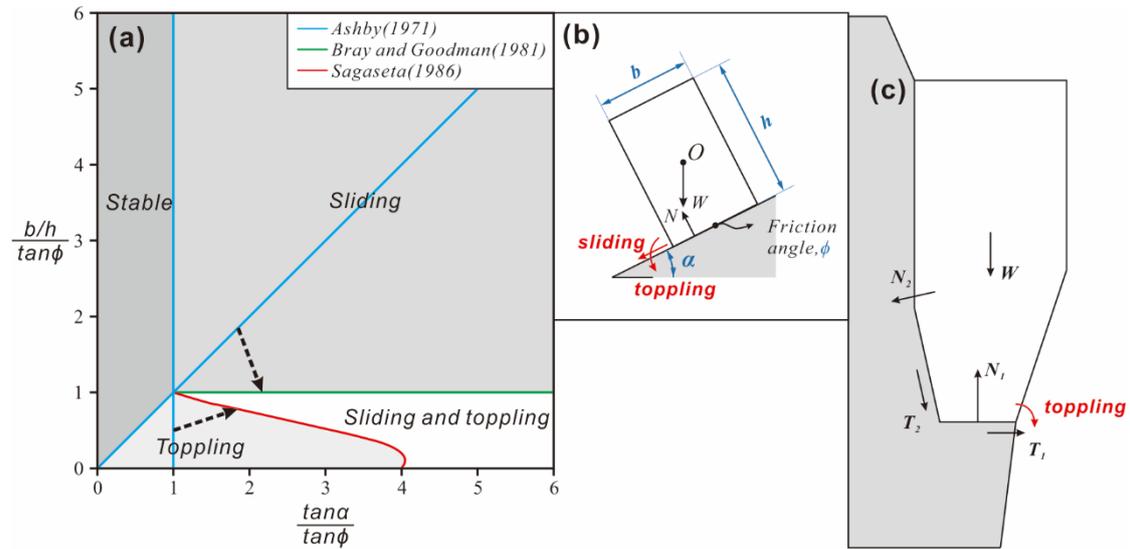
Figure 2 Traditional force analysis diagrams of the rock block. (a) and (b) are stability analysis diagrams of rock blocks under dynamic conditions, resting on an inclined plane with a dip angle of α. The rock block is generalized as a cuboid with dimensions $b \times h$ and weight W (as modified from Ashby (1971), Bray and Goodman (1981) and Sagaseta (1986)). (c) Force description of the toppling model proposed by Frayssines and Hantz (2009). In the above assumptions, N, T, and W are regarded as forces applied at a point.

The supporting force on the contact surface is assumed to be applied at a point in the current LEM methods (i.e., N in Fig. 2 b and c). However, the supporting force is actually a distributed force. The cavity generates an eccentricity effect on the overlying rock block and results in a non-uniform distribution of the supporting force on the contact surface, which is not considered in the traditional LEM. Furthermore, most studies simplified the three-dimensional geometry of the rock block by one cross-section, which is used to represent the critical features of the slope structure. Nevertheless, for natural blocks with basal cavities, the cavities usually present different depths along different directions (Pérez-Rey et al., 2021). Therefore, a three-dimensional model is necessary to calculate the accurate stability. In addition, when a block has multiple free faces and a complex structure, its potential failure is dominated by different modes, including rock mass damage and overall block failure. Therefore, the probable failure modes should be determined prior to the calculation of Fos.

Based on rockfall investigation in the Eastern Sichuan Basin, China, the main objective of this study was to propose a new three-dimensional method for the determination of failure modes and Fos of biased rockfall, considering the non-uniform force distribution on the contact surfaces. Compared with the traditional LEM method, this study takes into account the partial damage of the underlying soft rock and the overall instability of the overlying hard rock blocks, and can evaluate the stability of biased rockfall more comprehensively. Fos of the typical unstable rock blocks in the study area are calculated to validate the proposed method. In addition, the critical cavity retreat ratio in this area is analysed. This study is an extension of the basic LEM for rockfall, which can promote the accuracy of rockfall stability analysis and facilitate rockfall prevention and risk mitigation.

2 Study area

2.1 Geological setting

The study area is located on the northeastern edge of the Sichuan Basin, China (Fig. 3a). Continuous erosion processes generate moderate-low mountain and valley landforms (Yu et al., 2021). The tectonic structure of this area is characterized by a series of ENE anticlines and synclines (Fig. 3b, c). In the anticline area, the rock layers dip relatively steeply, where translational rockslides are the main mode of slope failure. The syncline area is dominated by gently dipping strata and is prone to rockfall (Zhou et al., 2018). The study area is located in the core of the Matouchang syncline, where the rock layers are sub-horizontal (Fig. 3d, e). In this valley, due to the longstanding fluvial incision, the relative relief is approximately 500 m and the valley flanks are extremely steep (Fig. 3e). In addition, the toes of the hill slopes are reshaped because of the construction of the G318 national road, which is the main traffic line and is always threatened by rockfalls dropping from steep rock slopes (shown in Fig. 3d and Table 1).
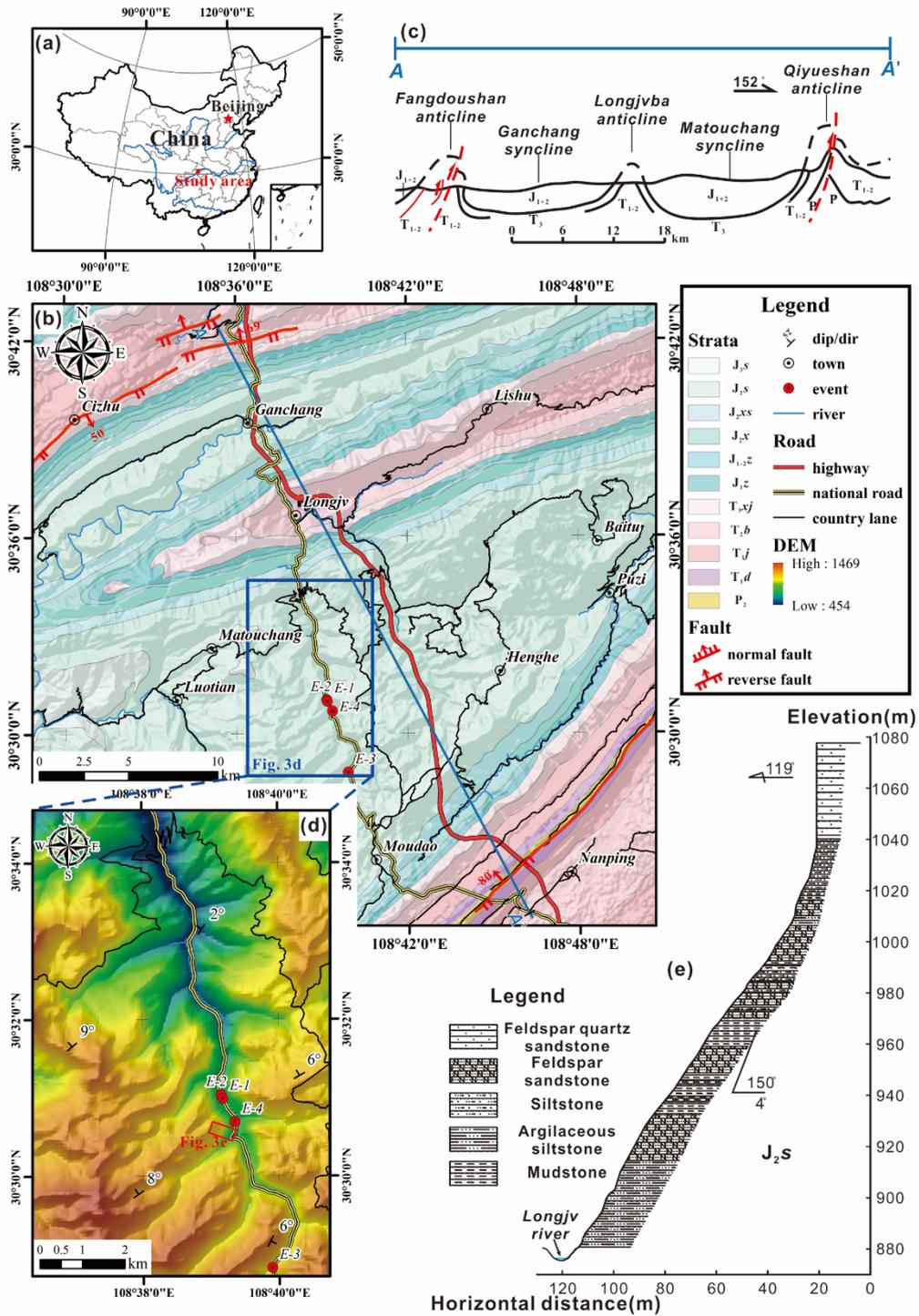
145

146 **Figure 3** (a) Location of the study area in China; (b) geological map of the study area; (c) tectonic sketch profile of A-A', whose location

147 is showed in Fig. 3b; (d) rockfall-prone segment and key investigation areas. The red dots are the positions of historical rockfall events,

corresponding to the numbers in Table 1; (e) Geological cross-section of the hillslope in the Jitougou section of G318 national road, which is marked by a red rectangle in Fig. 3d.

Table 1 Historical rockfall events along G318 national road in the study area

No	Location	Time of occurrence (GMT+8)	Volume [m³]	Consequence
E-1	K1698+900	2014-05 to 06*	Unknown	The power transmission facilities outside the road were smashed.
E-2	K1699+000	2015-02-14 23:00	About 240	A passing truck was stuck and two people dead.
E-3	K1690+700	2015-06-16	Unknown	The road was interrupted for a day.
E-4	K1698+400	2015-06-18 09:00	About 200	A vehicle was crashed into a gully and four people dead.

*Note: The exact time is unknown.

2.2 Rockfall characteristics

The slopes in the study area consist of a sub-horizontally interbedded sandstone and mudstone layer. Therefore, there are multiple layers of potentially unstable rock blocks in the hill slopes (Fig 4a). The thick sandstone has two sets of sub-vertical joints (Fig. 5), which cut the rock mass into blocks as the potential rockfall source (Fig. 4b). Cavities have formed in the underlying mudstone layer (Fig. 4c, d). Joints and bedding planes (BP) constitute the detachment surfaces between the blocks and steep slope (Fig. 4e). The eccentricity effect produced by the mudstone cavity plays an important role in the evolution process of rockfall. When the basal mudstone cannot provide adequate supporting force, the blocks detach from the steep slope, and biased rockfall occurs. Sliding and toppling are two possible failure modes of biased rockfall.

8
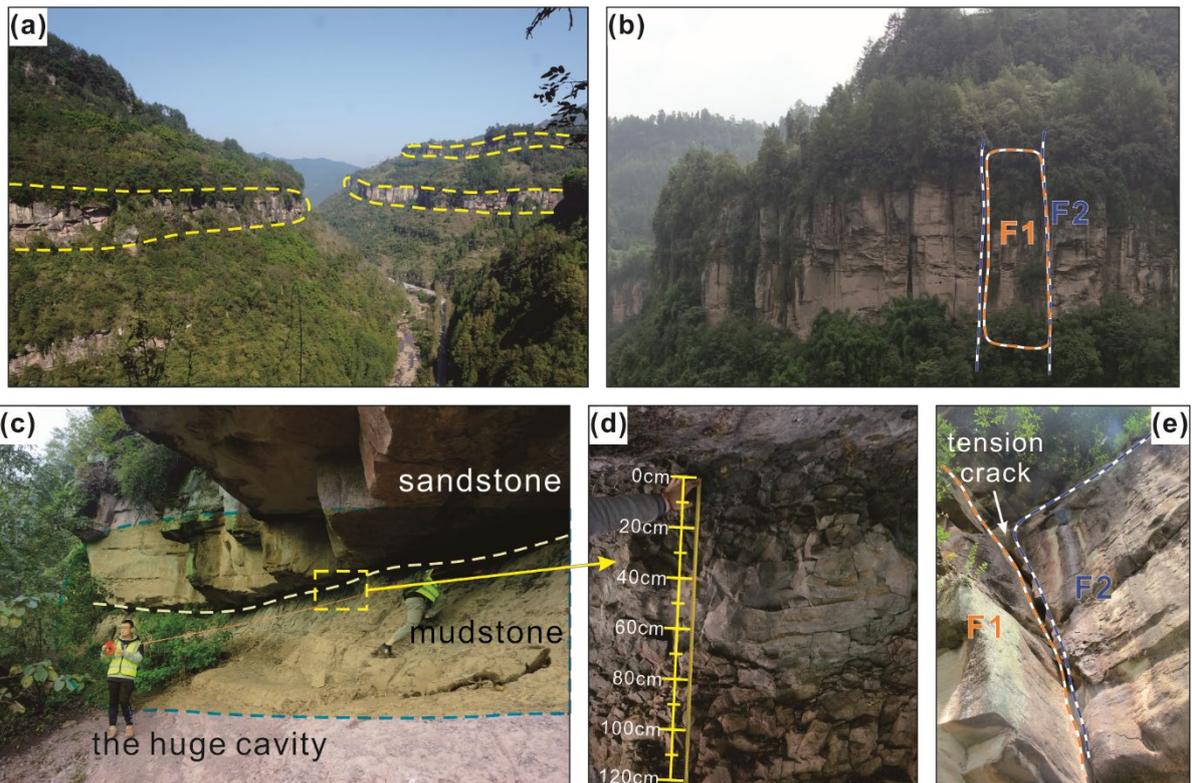
Figure 4 Characteristics of biased rockfalls in the study area. (a) Multiple-layers of rockfall sources, which is consist of thick sandstone. (b)
Two sets of sub-vertical joints (F1 and F2) recognized by the UAV photos. (c) Large basal cavity developed in the underlying mudstone.
(d) Dense fractures on the mudstone surface generated by weathering and compression. (e) Vertical tension crack in the rear of the block,
through which precipitation can infiltrate.

According to the historical rockfall events in this area, precipitation is considered a triggering effect of rock instability. The
precipitation mainly infiltrates along the sub-vertical joints or cracks of the sandstone (Fig. 4e). However, the drainage of
fissure water is hysteretic due to the obstruction of basal mudstone. Therefore, transient steady flow exists in vertical cracks
during heavy rainfall, and the hydrostatic pressure triggers the detachment of rock blocks. Thus, typical scenarios (such as
rainfall intensity and earthquake) need to be considered in the stability analysis model.
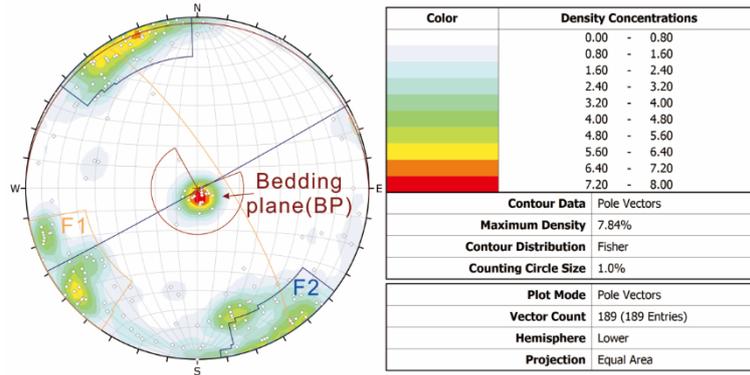
Figure 5 Stereo net produced using compass-clinometer survey data, which shows the densities and orientations of five clusters. The data
were collected in the rockfall-prone area shown in Fig. 3d.

3 Calculation method

3.1 Geological models and assumptions

A detailed geological investigation of unstable rock blocks was carried out in the study area (Fig. 6). The geological model
of the rock block is mainly composed of the overlying sandstone and the underlying mudstone. The sandstone block is
assumed to be a rigid body, which is divided by two sets of orthogonal vertical smooth joints without friction resistance.
According to the relatively persistent sub-vertical fractures observed in the field, the vertical joints are assumed to be fully
persistent in the geological model. The sandstone block is assumed to be a complete body without persistent discontinuity,
and it will not disintegrate before it falls. Due to the cavity in mudstone, the contact surface between sandstone and
mudstone exhibits an eccentricity effect where non-uniform stresses are distributed at different positions. Mudstone is
mainly loaded by compressive stress and tensile stress. When the compressive stress of mudstone exceeds its strength on the
outer side, some initial damage appears. The effective contact surface between mudstone and sandstone is reduced, which
aggravates the non-uniform distribution of stress. In this way, the ability of mudstone to resist the sliding and toppling of
overlying sandstone is reduced. In the field, compression deformation of mudstone can be observed, which usually manifests

as micro-fractures and cleavages (Fig. 4d). The deformation is very slight and slow in the short term. In addition, the LEM is essentially a force/stress approach that does not take into account the deformation. Therefore, in this study, it is assumed that the mudstone is not subjected to deformation. The rock block remains in the state of static equilibrium prior to the final overall failure. Fig. 7 displays the four evolution stages of biased rockfall. In the initial stage, the base cavity has not yet formed, and the normal force acting on the contact surface is uniform in different positions. The eccentricity effect leads to a non-uniform supporting force as the cavity grows, and partial damage gradually develops when the non-uniform stress exceeds the compressive or tensile strength of the mudstone. Under the triggering effects of rainfall or earthquakes, the rock blocks are separated by sliding or toppling.
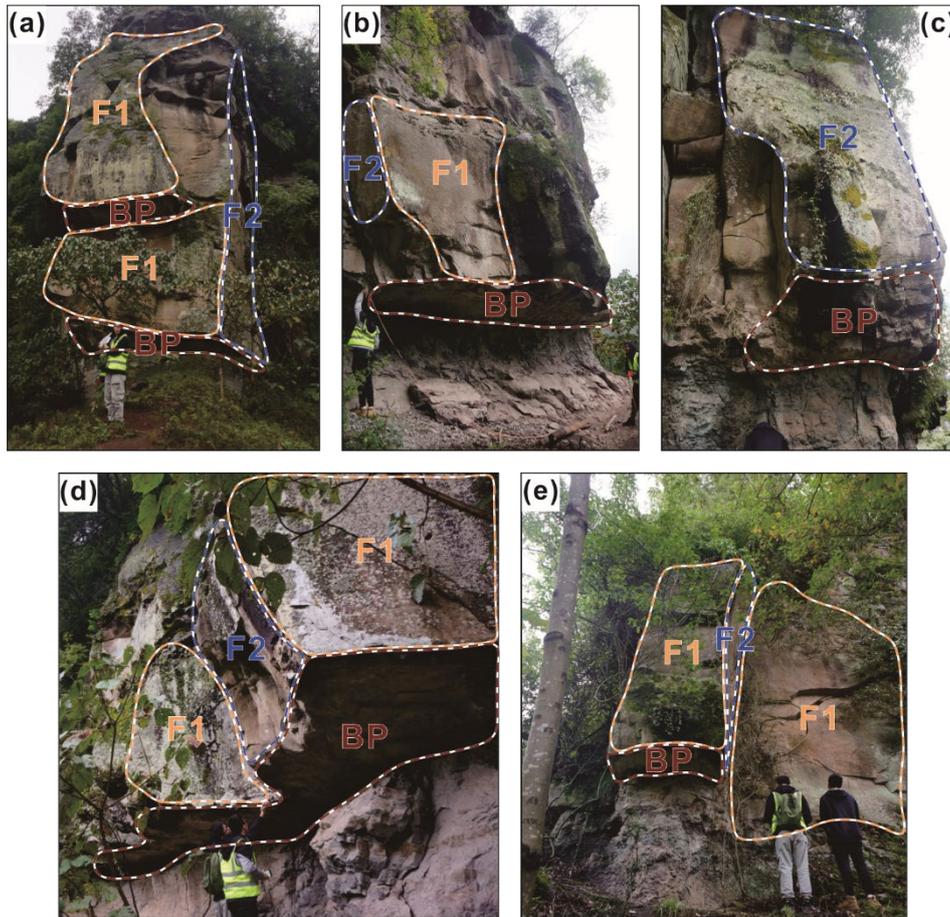

Figure 6 The unstable blocks were labelled W02, W08, W18, W04, and W21, which are detached by the dominating discontinuities in Fig. 5. Basal cavities can be identified under the bedding planes of sandstone.
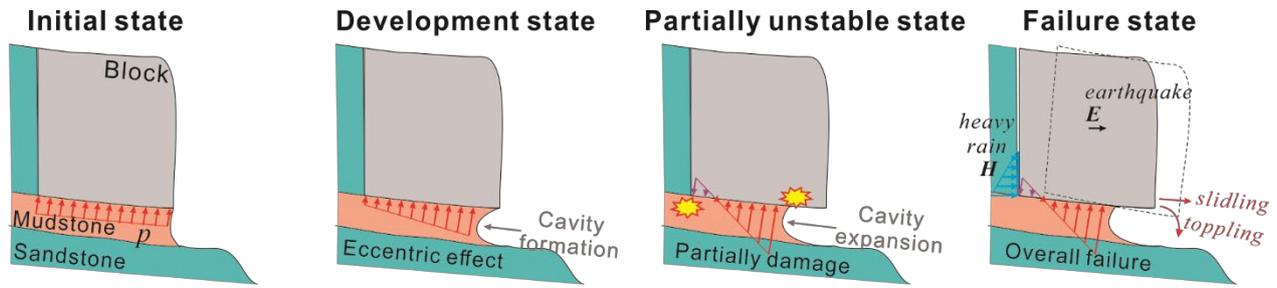
Figure 7 The evolution process of rock blocks from stable state to failure.

Fig. 8 represents the mechanical model of the force equilibrium analysis of a rock block with two or three free faces. The rock block (the overlying sandstone) is generalized as a parallelepiped block. The underlying mudstone is impermeable, so rainfall can fill the joints and transmit horizontal hydrostatic pressure. The shear strength of the underlying mudstone is assumed to obey the Mohr–Coulomb criterion. Rainfall and earthquakes decrease Fos by generating hydrostatic pressure H in the vertical crack and horizontal seismic force E on the block.

A Cartesian coordinate system is established in three-dimensional space for the force analysis. The origin O is located at the centre of the contact surface between sandstone and mudstone. For the case with two free surfaces, the orientation of the free surfaces is set to be the positive direction of the x-axis and y-axis. For the case with three free surfaces, the negative direction of the x-axis is also a free surface. Joint J2 is perpendicular to the x-axis, and joint J1 is perpendicular to the y-axis.
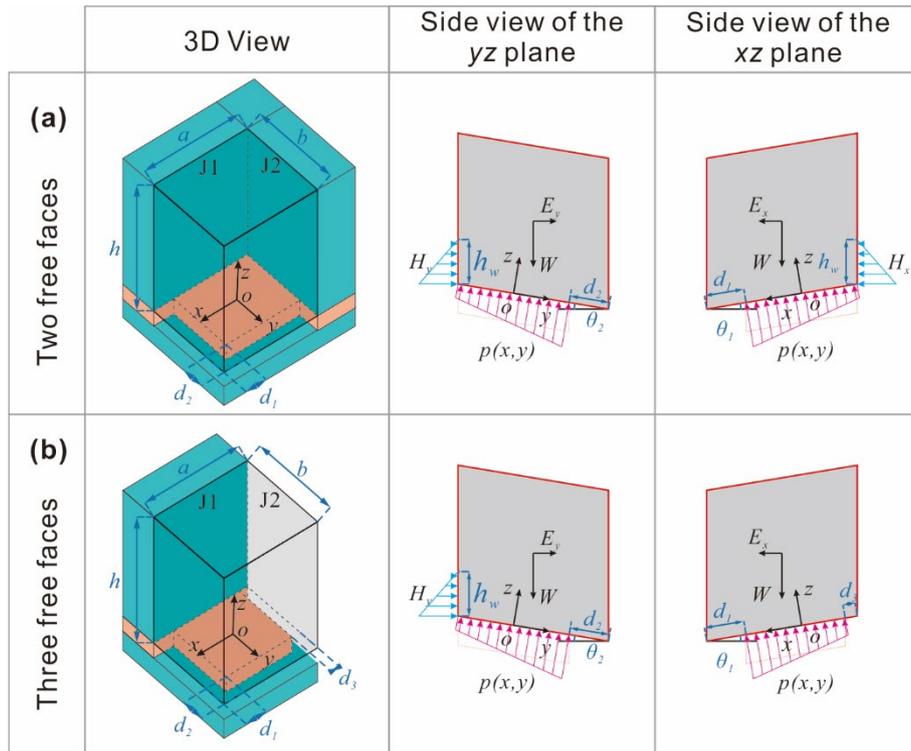
209   **Figure 8** Diagram of the force equilibrium analysis of the rock block model. (a) and (b) represent the case of unstable rock blocks with

210   two or three free vertical surfaces, respectively.

3.2 Calculation processes

211

3.2.1 Stress distribution at the block base

212

213   The following formulas are used to calculate the apparent dip of α (θ_1 and θ_2):

214
$$\theta_1 = \arctan(\tan \alpha \cdot \cos \omega_1) \tag{1}$$

215
$$\theta_2 = \arctan(\tan \alpha \cdot \cos \omega_2) \tag{2}$$

216   where ω_1 and ω_2 are the angles between the trend of the contact surface and the x direction or y direction, respectively.

217   As shown in Fig. 8b, with respect to the x-axis, gravity, seismic forces, and hydrostatic pressure create a non-symmetrical

218   stress distribution on the foundation. The bending moment of gravity with respect to the x-axis (M_{bWx}) is

219
$$M_{bWx} = W \cdot \frac{d_1 - d_3}{2} \cos \theta_1 \tag{3}$$

220   Assuming that the height of the water in the fracture is h_w, the hydrostatic pressure along the x direction (H_x) and its

221   bending moment (M_{bHx}) are respectively expressed as

222
$$H_x = \frac{\gamma_w h_w^2}{2}(b - d_2) \tag{4}$$

223
$$M_{bHx} = \int_{-\frac{b-d_2}{2}}^{\frac{b-d_2}{2}} \int_0^{h_w \cos \theta_1} \gamma_w \left(h_w - \frac{z}{\cos \theta_1}\right)\left(\frac{z}{\cos \theta_1} + \frac{a - d_1 - d_3}{2} \cdot \sin \theta_1\right) dz dy \tag{5}$$

224   The horizontal seismic force along x direction (E_x) and its bending moment (M_{bEx}) are respectively expressed as

225
$$E_x = k_e W \tag{6}$$

226
$$M_{bEx} = E_x \left(\frac{h}{2} - \frac{d_1 - d_3}{2} \sin \theta_1\right) \tag{7}$$

227   The total applied vertical load (N_z) and the total bending moments along the x direction (M_{bx}) can be derived as

228
$$N_z = W \cos \alpha - (H_x \cdot k_1 \cdot k_3 + E_x \cdot k_2) \sin \theta_1 - (H_y \cdot k_1 + E_y \cdot k_2) \sin \theta_1 \tag{8}$$

229
$$M_{bx} = M_{bWx} + M_{bHx} \cdot k_1 \cdot k_3 + M_{bEx} \cdot k_2 \tag{9}$$

230   where k_1, k_2 and k_3 are the coefficients set to make Eq. (8) and Eq. (9) compatible with different calculation scenarios.

231   Therefore, Eqs. (8) and (9) and the following formulas can be expressed in a unified form. In the natural scenario, k_1 and k_2

232   are both equal to 0. In the rainfall scenario, $k_1 = 1$. In the earthquake scenario, $k_2 = 1$. For the case of two free faces, $k_3 =$

233   1. For the case of three free surfaces, $k_3 = 0$.

234   Based on bending theory ([Adrian, 2010](#)), the eccentricity distance along the x direction (e_x) can be expressed as

235
$$e_x = \frac{M_{bx}}{N_z} = \frac{M_{bWx} + M_{bHx} \cdot k_1 \cdot k_3 + M_{bEx} \cdot k_2}{W \cos \alpha - (H_x \cdot k_1 \cdot k_3 + E_x \cdot k_2) \sin \theta_1 - (H_y \cdot k_1 + E_y \cdot k_2) \sin \theta_1} \tag{10}$$

236 The same method can be used to obtain e_y:

$$e_y = \frac{M_{by}}{N_z} = \frac{M_{bWy} + M_{bHy} \cdot k_1 + M_{bEy} \cdot k_2}{W \cos \alpha - (H_x \cdot k_1 \cdot k_3 + E_x \cdot k_2) \sin \theta_1 - (H_y \cdot k_1 + E_y \cdot k_2) \sin \theta_1} \quad (11)$$

238 According to the stress distribution of a rectangular shaped foundation (Adrian, 2010), the stress in the (x, y) coordinates,
239 $p(x, y)$, is

$$p(x, y) = \frac{N}{A} + \frac{N e_x}{I_y} x + \frac{N e_y}{I_x} y \quad (12)$$

241 with the formulas

$$I_x = \frac{(a - d_1)(b - d_2)^3}{12} \quad (13)$$

$$I_y = \frac{(b - d_2)(a - d_1)^3}{12} \quad (14)$$

$$A = (a - d_1 - d_3)(b - d_2) \quad (15)$$

245 By substituting Eq. (13-15) into Eq. (12), $p(x, y)$ can be derived as

$$p(x, y) = \frac{N}{A}\left[1 + \frac{12 e_x}{(a - d_1 - d_3)^2} x + \frac{12 e_y}{(b - d_2)^2} y\right] \quad x \in \left[-\frac{a - d_1 - d_3}{2}, \frac{a - d_1 - d_3}{2}\right], y \in \left[-\frac{b - d_2}{2}, \frac{b - d_2}{2}\right] \quad (16)$$

247 p_{max} and p_{mim} can be derived from Eq. (16) as

$$p_{max} = p\left(\frac{a - d_1 - d_3}{2}, \frac{b - d_2}{2}\right) \quad (17)$$

$$p_{min} = p\left(-\frac{a - d_1 - d_3}{2}, -\frac{b - d_2}{2}\right) \quad (18)$$

250 The mudstone foundation has both compressive strength and tensile strength, so the value of $p(x, y)$ is modified to obtain
251 the two piecewise functions

$$p_p(x, y) = \begin{cases} \sigma_{cmax}, & p(x, y) \geq \sigma_{cmax} \\ p(x, y), & 0 < p(x, y) \leq \sigma_{cmax} \\ 0, & p(x, y) < 0 \end{cases} \quad (19)$$

$$p_n(x, y) = \begin{cases} 0, & p(x, y) < -\sigma_{tmax} \\ p(x, y), & -\sigma_{tmax} \leq p(x, y) < 0 \\ 0, & p(x, y) \geq 0 \end{cases} \quad (20)$$

254 Here, $p_p(x, y)$ provides support normal force for the overlying sandstone, and $p_n(x, y)$ provides tension force.

255 **3.2.2 Calculation of factors of safety**

256 According to the principle of friction, the ultimate shear strength τ_{max} is

$$\tau_{max} = \int_{-\frac{a - d_1 - d_3}{2}}^{\frac{a - d_1 - d_3}{2}} \int_{-\frac{b - d_2}{2}}^{\frac{b - d_2}{2}} \left[p_p(x, y) \tan \varphi + c\right] dy\, dx \quad (21)$$

258 Therefore, Fos against sliding, Fos_{sl}, can be defined as

259 $$Fos_{sl} = \frac{S_{stabilizing}}{S_{sliding}} = \frac{\tau_{max}}{W|\sin\alpha_s| + H_x \cdot \cos\omega_s \cdot \cos\alpha_s \cdot k_1 \cdot k_3 + H_y \cdot |\sin\omega_s| \cdot \cos\alpha_s \cdot k_1 + E \cdot \cos\alpha_s \cdot k_2} \tag{22}$$

260 When the block can slide freely, $\alpha_s = \alpha$, $\omega_s = 0$; when the block is constrained to slide along a joint plane (e.g., J1), $\alpha_s =$

261 θ_1 or θ_2, $\omega_s = \omega_1$ or ω_2. For the case of an anaclinal slope, the sliding direction is opposite to the free surface. Therefore,

262 the rock block does not slide, and Fos_{sl} is not considered in the model.

263 With regard to stability against toppling, along the x direction, the part of the block above the mudstone base provides the

264 stabilizing moment $M_{W_{inx}}$, and the part of the block above the cavity provides the overturning moment $M_{W_{outx}}$. When

265 tension exists, there is an additional stabilizing moment. M_{px}, $M_{W_{inx}}$, $M_{W_{outx}}$ and M_{px} can be derived as

266 $$M_{W_{inx}} = W\frac{a - d_1}{a}\cos\theta_1 \cdot \left(\frac{a - d_1}{2}\right) \tag{23}$$

267 $$M_{W_{outx}} = W\frac{d_1}{a}\cos\theta_1 \cdot \frac{d_1}{2} \tag{24}$$

268 $$M_{px} = -\int_{-\frac{b-d_2}{2}}^{\frac{b-d_2}{2}}\int_{\frac{a-d_1-d_3}{2}}^{\frac{a-d_1-d_3}{2}} p_n(x,y) \cdot \left(\frac{a}{2} - d_1 - x\right) dx\, dy \tag{25}$$

269 and M_{Hx} and M_{Ex} can be derived as

270 $$M_{Hx} = \int_{-\frac{b-d_2}{2}}^{\frac{b-d_2}{2}}\int_0^{h_w\cos\theta_1} \gamma_w\left(h_w - \frac{z}{\cos\theta_1}\right)\left(\frac{z}{\cos\theta_1} + (a - d_1)\sin\theta_1\right) dz\, dy \tag{26}$$

271 $$M_{Ex} = E_x\left(\frac{h}{2} + \left(\frac{a}{2} - d_1\right)\sin\theta_1\right) \tag{27}$$

272 Therefore, the Fos against toppling along the x direction, Fos_{tox}, results in

273 $$Fos_{tox} = \frac{M_{stabilizing}}{M_{overturning}} = \frac{M_{W_{inx}} + M_{px}}{M_{W_{outx}} + M_{Hx} \cdot k_1 \cdot k_3 + M_{Ex} \cdot k_2} \tag{28}$$

274 Similarly, Fos_{toy} can be obtained as

275 $$Fos_{toy} = \frac{M_{stabilizing}}{M_{overturning}} = \frac{M_{W_{iny}} + M_{py}}{M_{W_{outy}} + M_{Hy} \cdot k_1 + M_{Ey} \cdot k_2} \tag{29}$$

276 The smaller value is selected as the Fos of the toppling failure mode Fos_{to}:

277 $$Fos_{to} = min(Fos_{tox}, Fos_{toy}) \tag{30}$$

278 When the stress on mudstone exceeds its strength, it causes partial damage and decreases the stability of the rock block.

279 Therefore, Fos with the consideration of compressive strength (Fos_{co}) and tensional strength (Fos_{te}) can be derived as

280 $$Fos_{co} = \frac{\sigma_{cmax}}{p_{max}} \tag{31}$$

281 $$Fos_{te} = \frac{\sigma_{tmax}}{-p_{min}} \tag{32}$$

282   Fos_{co} and Fos_{te} represent the current damage degree of mudstone due to compressive stress and tensile stress, respectively.

283   When the stress exceeds the ultimate strength, the strength of the mudstone is reduced to the residual value, and the initial

284   deformation appears. The ability of mudstone to provide resistance to the sliding and toppling of sandstone blocks is thus

285   reduced, and Fos_{sl} and Fos_{to} subsequently decline. The smaller the value of Fos_{co} and Fos_{te}, the greater the damage to the

286   underlying mudstone. The effective contact area between sandstone and mudstone becomes smaller as the development of

287   compressive and tension damage, which significantly affects the stability of the overlying sandstone block.

288   Finally, four Fos of unstable rock block are obtained. Fos_{sl} and Fos_{to} are routine indicators directly representing the

289   stability of sandstone blocks. Fos_{co} and Fos_{te} are two indicators proposed in this study for the stability analysis of biased

290   rockfall, which describe the damage state of the underlying mudstone base. It is necessary to simultaneously consider four

291   Fos to evaluate the stability of unstable biased rockfall. The entire calculation process is shown in Fig. 9.
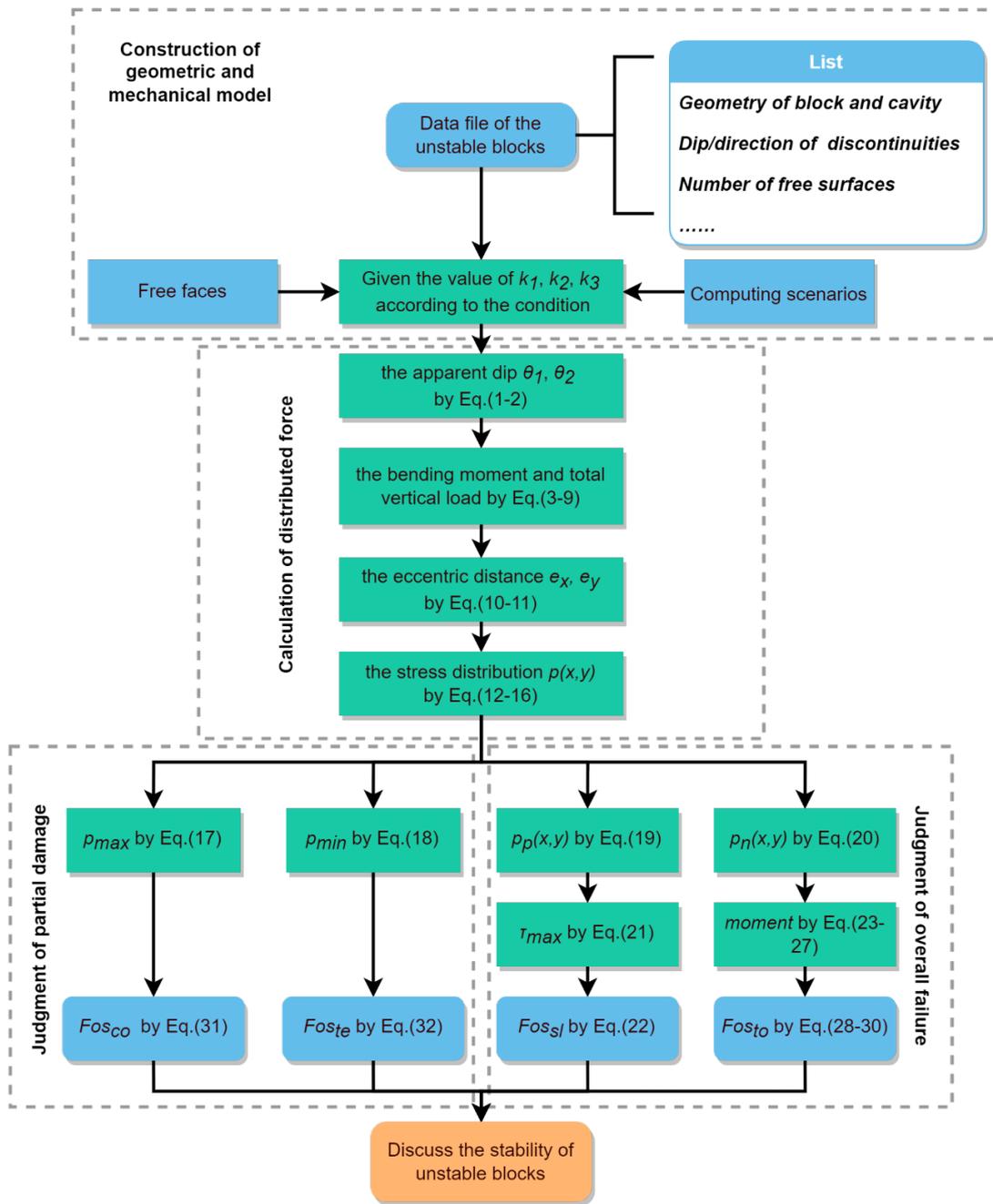
Figure 9 Calculation process of Fos of the unstable rock blocks.

4 Parameters and results

296   A detailed field investigation was carried out in the source area of rockfall (Fig. 3d). The size of the blocks was determined

297   by on-site measurement with tape and a laser rangefinder. The basal cavities in mudstone were measured with a steel ruler,

298   and the morphological characteristics of mudstone foundation were mainly described with the average erosion depth of the

299   cavity. The attitude of discontinuities was measured by compass. The mechanical parameters for the Fos calculation of rock

300   blocks were determined by referring to published literature and investigation reports in this area. The unit weight of the

301   sandstone block (γ_s) is 25 kN/m^3 (Tang et al., 2010), the friction angle of the contact surface (φ) is set to 25° and the

302   cohesion (c) is set to 70 kPa (Zhang et al., 2016). Because of the strength degradation of mudstone foundations due to

303   intense weathering, the maximum compressive stress of mudstone (σ_{cmax}) is replaced by the bearing capacity of mudstone

304   foundations (2300 kPa), which is obtained through plate load tests in adjacent areas (Zheng et al., 2021). In addition, the

305   maximum tensile stress of mudstone (σ_{tmax}) is value as one-ninth of σ_{cmax}. The height of the water level (h_w) is set to be

306   one-third of h, and an earthquake contribution coefficient k_e of 0.05 is considered in stability calculations. The data obtained

307   from the field survey were organized according to the coordinate system of the geological model in Section 3.1, and Fos was

308   calculated according to the calculation steps in Section 3.2. The calculated geometric parameters and Fos results are shown

309   in Table 2.

310 **Table 2** Geometric parameters of rock blocks in the study area and Fos results.

Block number	Free faces	h [m]	a [m]	b [m]	d_1 [m]	d_2 [m]	d_3 [m]	α [°]	Dip direction [°] BD	J1	J2	NS (Natural scenario) Fos_{te}	Fos_{co}	Fos_{sl}	Fos_{to}	Fos_{min}	RS (Rainfall scenario) Fos_{te}	Fos_{co}	Fos_{sl}	Fos_{to}	ES (Earthquake scenario) Fos_{te}	Fos_{co}	Fos_{sl}	Fos_{to}
W01	3	23	7.2	6.1	0.65	0.25	0.17	6	78	7	97	-	2.99	5.61	101.54	2.99	-	2.56	3.18	11.91	0.90	1.63	3.81	4.88
W02	3	23	6.42	5.25	0.78	0.4	0.31	16	148	51	141	-	2.84	2.10	52.28	2.10	-	2.33	1.54	8.49	0.51	1.48	1.82	3.79
W03	2	20	3.5	2.6	0.84	0.55	-	7	341	53	143	0.52	1.56	16.53	4.72	0.52	0.15	0.86	2.83	1.02	0.14	0.81	9.12	1.01
W04	2	19	4.6	4.6	0.62	0.77	-	7	273	65	155	7.35	2.37	-	24.74	2.37	0.80	1.81	-	6.83	0.35	1.38	-	3.23
W05	2	15	16.7	5.6	2.13	1.36	-	5	283	50	140	1.70	2.57	-	9.86	1.70	1.19	2.39	-	6.10	0.63	1.99	-	3.36
W06	3	20	16.7	9.7	7.5	4.2	3.9	5	302	226	316	0.15	0.87	8.67	1.53	0.15	0.15	0.84	4.73	1.52	0.12	0.72	5.96	1.16
W07	2	22	9.2	3.7	0.64	0.8	-	12	324	315	405	-	2.27	2.82	22.86	2.27	0.57	1.55	1.62	2.97	0.34	1.28	2.44	2.21
W08	2	23	12	7.9	2	1.9	-	3	317	332	422	0.76	1.55	11.75	8.99	0.76	0.51	1.40	4.51	5.09	0.29	1.14	6.29	2.84
W09	2	18	8.4	6	0.9	2.5	-	8	60	335	425	0.38	1.48	4.98	2.23	0.38	0.29	1.30	2.87	1.56	0.22	1.12	4.08	1.20
W10	2	23	5.7	3.3	1.3	0.85	-	5	329	313	403	0.30	1.16	7.41	2.53	0.30	0.12	0.71	2.30	0.71	0.11	0.68	5.84	0.75
W11	3	22	1.1	2	0.1	0.64	0.1	4	327	120	210	1.13	1.74	19.08	4.97	1.13	0.12	0.69	2.37	0.51	0.07	0.49	10.57	0.73
W12	2	25	3.9	4	0.74	0.96	-	12	355	297	387	0.64	1.44	2.78	10.36	0.64	0.15	0.82	1.48	1.81	0.14	0.75	2.70	1.61
W13	2	12	11.9	10.9	3	2.28	-	7	36	73	163	1.06	2.77	7.28	9.39	1.06	0.99	2.71	5.63	9.02	0.70	2.41	4.93	5.65
W14	3	19	13	5	0	1.1	0	8	296	73	163	-	2.67	6.40	12.57	2.67	3.75	2.28	3.09	5.15	0.68	1.75	4.41	2.94
W15	2	18	22	6	8.3	0	-	8	351	200	290	0.70	1.84	9.74	2.93	0.70	0.60	1.75	5.03	2.83	0.39	1.50	5.79	2.34
W16	3	11	5.2	7.6	0	2.9	0	13	42	144	234	1.09	3.04	3.46	3.65	1.09	1.01	2.96	2.84	3.45	0.62	2.45	2.98	2.45
W17	3	7	8	2	0	0.56	0	20	30	156	246	7.71	6.72	3.07	6.83	3.07	3.40	5.87	2.29	4.49	1.48	4.70	2.81	2.86
W18	2	12	8.5	4.5	1.61	1.27	-	2	252	253	343	0.97	2.66	20.49	7.05	0.97	0.75	2.46	10.06	4.50	0.50	2.08	8.90	2.82
W19	2	15	4.2	5.2	1.6	0.68	-	5	28	56	146	0.75	2.12	8.71	5.49	0.75	0.48	1.80	4.17	3.66	0.31	1.48	5.79	2.24
W20	3	15	1.8	1.7	0.23	0.5	0.3	4	20	63	153	7.96	2.95	9.44	6.08	2.95	0.29	1.43	3.39	0.87	0.18	1.07	7.12	1.03
W21	3	20	18.9	9	0	2	0	7	348	71	161	-	2.51	4.96	12.25	2.51	-	2.36	3.31	7.48	1.15	1.90	3.58	3.95
W22	2	7	5.4	5.7	1	1.65	-	6	294	53	143	1.53	4.48	-	5.78	1.53	1.44	4.38	-	5.37	1.00	3.81	-	3.88

311 Note: When there is no tensile stress in the mudstone foundation, Fos_{te} has no value. For the case of an anaclinal slope, blocks do not slide and Fos_{sl} has no value. Both parameters are replaced by "-".

5 Discussion

5.1 Characteristics of rock block stability

There are up to 12 results of Fos per potential unstable block with the consideration of three scenarios and four failure modes (i.e., partial damage and overall failure). Most Fos_{te} values are less than 1 in all scenarios (purple points in Fig.10), except for two blocks (i.e., W17 and W20), whose Fos_{te} values are also close to 1 under rainfall or earthquake scenarios. Although most of Fos_{co} values (green points in Fig. 10) are greater than 1, they are closer to the critical state of $Fos = 1$ than Fos_{sl} and Fos_{to} (represented by blue and yellow points in Fig. 10, respectively). The compression damage of the exposed mudstone can be investigated in the field survey (Fig. 4d). However, it is difficult to observe the phenomenon of tensile damage inside the mudstone base. In the case of weak tensile strength, the mudstone base suffers from tensile failure, and compression failure usually occurs before tension failure. According to the results, their Fos_{te} and Fos_{co} are less than 1 or close to 1, which means that the underlying mudstone has been partially damaged due to slight compressive or tensile failure, and the blocks are potentially unstable with the current depth of the basal cavity. However, most of the blocks do not exhibit overall failure, and they still exist on the slope. Moreover, their Fos_{sl} and Fos_{to} values are greater than 1 in different scenarios, which is consistent with this actuality. The results indicate that most of the blocks are close to a critical state, in which they are partially damaged but the whole block is still stable.
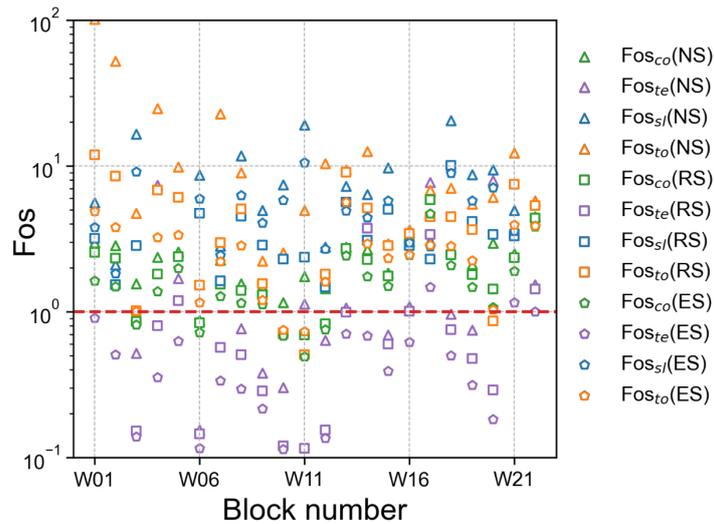

Figure 10 Distribution of Fos in different scenarios. Shapes represent different scenarios and colours represent different failure modes.

5.2 Relationship between Fos and geometric parameters

Fig. 11 presents the relationship between Fos_{min} and two main geometric parameters, the dip of the contact surface and the retreat ratio. In general, the dip angle of the contact surface (α) is the key factor influencing the sliding failure mode. The

19

horizontal axis in Fig. 11a is α between the rock blocks and underlying mudstone. Most of the points in Fig. 11a are in the interval [0, 8°], which is consistent with the features of sub-horizontal strata in the study area. The shade of the points does not change significantly in the x-axis direction, as Fig. 11a shows. Therefore, compared with the maximum retreat ratio (r_{max}), the dip of the contact surface has less influence on rockfall stability in the study area. There was a significant positive correlation between the retreat ratio (r_{max}) and Fos_{min}. In Fig. 11b, as the retreat ratios increase in the positive direction of the x-axis and y-axis, the rock blocks show a notable tendency to be unstable.
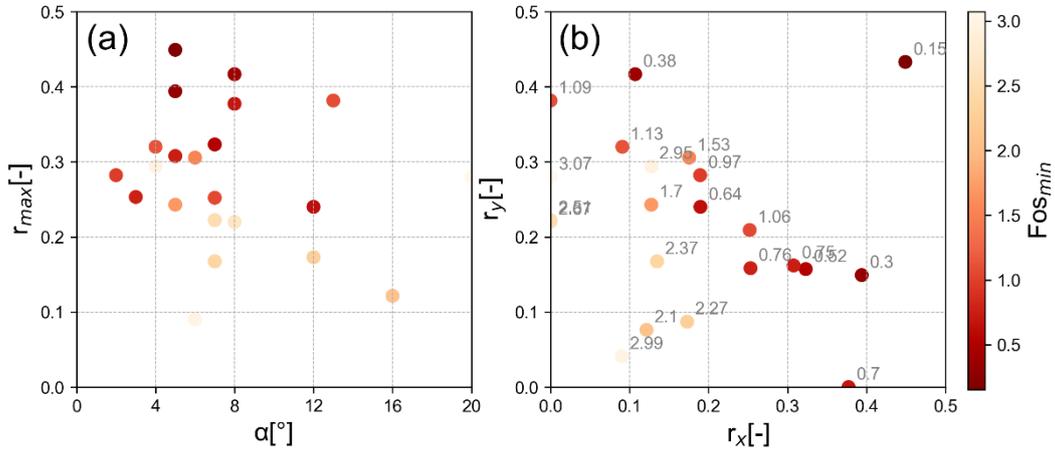
Figure 11 Correlation between Fos and the dip of contact surface and retreat ratio. Here, α is the dip angle of the contact surface between rock block and underlaying mudstone, r_x and r_y are the retreat ratio along x direction and y direction, respectively, equal to d_1/a and d_2/b, and r_{max} is the larger of r_x and r_y.

5.3 Definition of rockfall susceptibility

To explore the variation in Fos with the progressive erosion process of the cavity on the blocks, the cavity retreat velocities in different directions are assumed to be equal (5 mm/year, Zhang et al. (2016)). Fig. 12 shows the variations in Fos of two specific blocks during the evolution process of the mudstone cavity. In the initial stage, the cavity is small, and the overlying block is stable; all Fos values are greater than 1.0. The cavity expands over time as the mudstone weathers; then, the contact area decreases, and non-uniform distributed stress arises. When the stress exceeds the ultimate strength of mudstone in a partial area, Fos_{co} and Fos_{te} decrease significantly, as shown in Fig. 12. The instability of the blocks starts from the failure (or damage) of the foundation. Fos_{te} and Fos_{co} reach the critical state much earlier than Fos_{sl} and Fos_{to}. For these two specific blocks, when r_{max} increases to 0.4, Fos_{sl} and Fos_{to} are still higher than 1.0. This means that the rock blocks can remain globally stable in this condition.

These results further elucidate the stability analysis model proposed in this study. Fos_{co} and Fos_{te} introduced in this model present the damage state of basal mudstone caused by compressive and tensile stresses, which do not provide global instability of the overlying block as sliding and toppling. However, Fos_{co} and Fos_{te} are important preliminary signs of

subsequent global failure of the rock block. The damage in the basal mudstone can significantly accelerate weathering and prompt expansion of the cavity, which will lead to global failure. The lower Fos_{co} and Fos_{te} are, the lesser the safety margin of the blocks. Therefore, the four Fos used in this study can provide a more comprehensive quantification of rockfall stability.

This result is consistent with Fig. 10, in which 63.7% of the purple and green points (Fos_{te} and Fos_{co}) are located between $Fos = 0.7$ and $Fos = 2.0$. This result can be validated by the field phenomena. In the study area, rock damage (e.g., micro-fractures and cleavages) can be observed in the underlying mudstone. However, most overlying rock blocks are stable at the present time. This means that even if Fos_{sl} or Fos_{to} is higher than 1, its foundation has begun to be damaged. In the case of heavy rain or earthquakes, Fos_{sl} and Fos_{to} may be reduced to less than 1, and the rockfall occurs.
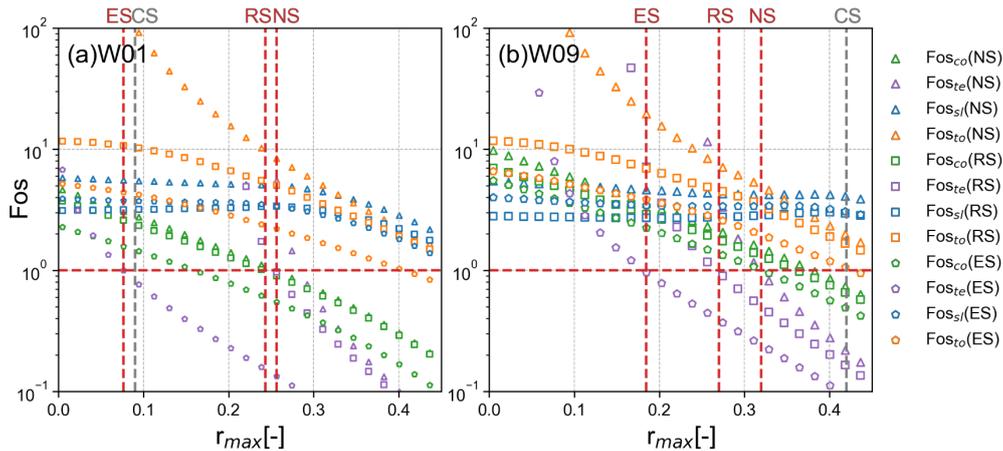
Figure 12 Variation in Fos with r_{max}. (a) and (b) are the results for W01 and W09, respectively, which represent the situation of the blocks with two and three free faces. The grey dotted line (CS) approximately represents the current state of the unstable blocks. The red dotted lines correspond to the critical values of r in different scenarios.

Based on the meaning of four Fos, rockfall susceptibility can be divided into three levels. When both Fos_{co} and Fos_{te} are greater than 1, the overall rock block is stable, and the mudstone base is not damaged, which is defined as "low susceptibility" and represented by the green area in Fig. 13. With the development of cavity erosion, when Fos_{co} or Fos_{te} is less than 1 and Fos_{sl} and Fos_{to} are higher than 1, the base undergoes be damaged, and the overlying sandstone blocks remain relatively stable. This state is defined as "moderate susceptibility" and represented by the orange area. When Fos_{sl} or Fos_{to} is less than 1 in some scenarios, the rock blocks are in a "high susceptibility" state, which means that rockfalls are highly likely to occur. Fig. 13a indicates that along with the increase in the cavity retreat ratio, the susceptibility of W01 and W09 changes from low susceptibility to moderate susceptibility in the natural scenario. As Fig. 13b and c show, when rainfall or earthquake occurs, Fos_{sl} or Fos_{to} of some blocks is less than 1, which means that some blocks have evolved to the state of high susceptibility and the overall sandstone blocks are unstable.
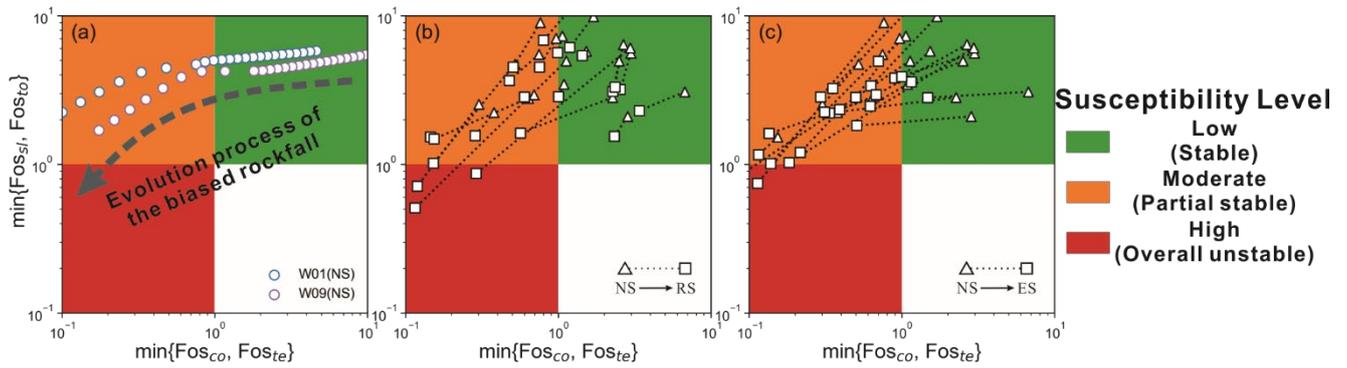
Figure 13 Rockfall susceptibility based on the combination of four *Fos*. The susceptibility is defined as three levels, represented by red, orange and green. (a) shows the progressive failure process of the rock block changing from low susceptibility to moderate susceptibility as the cavity retreat ratio increases (illustrated by W01 and W09 in the natural scenario. (b) and (c) show the change in susceptibility of biased rock blocks, when the scenario changes from natural conditions to rainfall and earthquake conditions.

5.4 Critical retreat ratio in the study area

The cavity plays an important role in the progressive failure process of biased rockfall. To analyse the effect of the retreat ratio on the stability of rock blocks, all blocks in the study area were selected to calculate their *Fos* and susceptibility level with the increasing r, whose retreat velocities in different directions are assumed to be equal. Fig. 14 shows that along with the increase in the retreat ratio, the susceptibility level of rock blocks changes from low to moderate susceptibility. Corresponding to the critical state of $\min\{Fos_{co}, Fos_{te}\} = 1$ of all blocks, the minimum retreat ratio is 0.26, and the maximum retreat ratio is 0.41, as marked by the vertical grey dotted line in Fig. 14. According to the statistical analysis of critical retreat ratios, both mean and median are 0.33. Therefore, the critical retreat ratio of the rock blocks in the study area can be determined as 0.33, which is marked by the vertical red dotted line in the Fig. 14. The critical retreat ratio calculated by this method can be used for the preliminary identification of potential unstable rock blocks in a specific area, which can help concentrate limited risk treatment resources on these priorities. It should be emphasized that the mechanical parameters and analysis scenarios significantly affect the critical value. Therefore, the elaborative risk control of a given rockfall should be arranged based on its specific parameters and analysis scenarios.
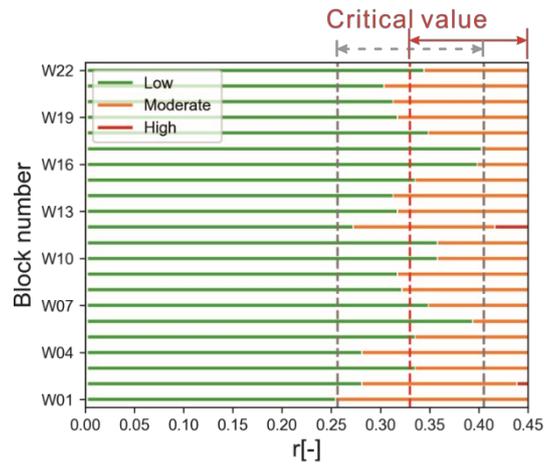
396

397 **Figure 14** Effect of the retreat ratio (r) on the Fos of the rock block, which is illustrated by all blocks in the study area.

398 **5.5 Limitations**

399 This study involves the development of an analytical model for the three-dimensional stability of biased rockfall, combining

400 the basic LEM method and the consideration of the eccentricity effect. Due to the complexity of rock structure and force

401 analysis, it is necessary to highlight the limitations of this model.

402 First, this study uses a three-dimensional coordinate system and bending theory. It is difficult to consider diverse shapes of

403 rock blocks, and the rock block was simplified as a prismatic column. The assumption of fully persistent discontinuities may

404 underestimate the stability of rock blocks, and ignores the stress transmission in joints or rock bridges. Then, following the

405 basic framework of the general LEM method, this study assumed that the rock is not subjected to deformations. The

406 complete stress–strain behaviour, such as the deformation in the mudstone layer, is not considered in this study. Furthermore,

407 the block stability is strongly influenced by the uncertainty of mechanical parameters. However, because of the difficulties in

408 sampling strongly weathered mudstone, it is difficult to obtain adequate parameter values for uncertainty statistics. These

409 limitations will be important considerations in future studies.

410 **6 Conclusion**

411 Due to differential weathering in sub-horizontally interbedded of hard rock and soft rock, multi-layer biased rockfalls

412 develop on steep slopes. In mountainous ranges, cut slopes, and coastal cliffs, rockfall may cause significant facility damage

413 and casualties in residential areas and transport corridors. The aim of this study was to present a new three-dimensional

414 analytical method for the stability of rock blocks with basal cavities. In this method, a non-uniform distributed stress due to

415 the eccentricity effect is applied at the contact surface instead of a point force. The method considers four failure modes

416 according to the rockfall evolution process, including partial damage of the soft foundation (Fos_{co} and Fos_{te}) and overall

417 failure of the rock block (Fos_{sl} and Fos_{to}).

23

418 Taking the northeast edge of the Sichuan Basin in Southwest China as the study area, the proposed method is used to
419 calculate the *Fos* of biased unstable rock blocks. The results show that in the natural scenario, the underlying mudstone of
420 some rock blocks has been partially damaged, and compression failure of the mudstone has been observed in the field. Some
421 rock blocks are expected to fail as a whole in rainfall or earthquake scenarios. The statistical analysis indicates that the
422 retreat ratio is the crucial factor influencing the *Fos* of biased rockfall. On the basis of different combinations of four *Fos*,
423 rockfall susceptibility was classified into three levels. As the retreat rate increases, the rock blocks undergo an evolution
424 process from stability to partial instability and then overall instability. Based on the current mechanical parameters of the
425 eastern Sichuan Basin, the critical retreat ratio from low to moderate rockfall susceptibility is 0.33.

426 The proposed method improves the three-dimensional mechanical model of a rock block with a basal cavity by considering
427 non-uniform distributed stress at the contact surface, which could promote the accuracy of rockfall stability analysis. Due to
428 the assumptions adopted and the complexity of the failure mechanism of biased rockfall, there are some limitations in this
429 method, mainly including the simplification of boundary conditions and rock deformation. These limitations will be
430 important considerations in future studies.

431 **Data availability**

432 All raw data can be provided by the corresponding authors upon request.

433 **Author contributions**

434 XS, BC and JD planned the campaign; XS and BC performed the field measurements; XS, BC, WW and BL designed and
435 developed the methodology. XS, BC and JD analysed the data; XS and BC wrote the manuscript draft; JD and WW
436 reviewed and edited the manuscript.

437 **Competing interests**

438 The authors declare that they have no conflicts of interest.

References

Adrian, I.: Pressures distribution for eccentrically loaded rectangular footings on elastic soils, Proceedings of the 2010 international conference on Mathematical models for engineering science, Tenerife, Spain, 213–216,

Alejano, L. R., Carranza-Torres, C., Giani, G. P., and Arzua, J.: Study of the stability against toppling of rock blocks with rounded edges based on analytical and experimental approaches, Eng. Geol., 195, 172-184, https://doi.org/10.1016/j.enggeo.2015.05.030, 2015.

Alejano, L. R., Ordóñez, C., Armesto, J., and Rivas, T.: Assessment of the instability hazard of a granite boulder, Nat. Hazards, 53, 77-95, https://doi.org/10.1007/s11069-009-9413-0, 2010.

Ashby, J.: Sliding and toppling modes of failure in models and jointed rock slopes, M.S. thesis, Imperial College London University, London, 1971.

Bray, J. W. and Goodman, R. E.: The theory of base friction models, Int. J. Rock Mech. Min. Sci. Geomech. Abstr., 18, 453-468, https://doi.org/10.1016/0148-9062(81)90510-6, 1981.

Budetta, P.: Assessment of rockfall risk along roads, Nat. Hazards Earth Syst. Sci., 4, 71-81, https://doi.org/10.5194/nhess-4-71-2004, 2004.

Budetta, P. and Nappi, M.: Comparison between qualitative rockfall risk rating systems for a road affected by high traffic intensity, Nat. Hazards Earth Syst. Sci., 13, 1643-1653, https://doi.org/10.5194/nhess-13-1643-2013, 2013.

Chau, K. T., Wong, R. H. C., Liu, J., and Lee, C. F.: Rockfall hazard analysis for Hong Kong based on rockfall inventory, Rock Mech. Rock Eng., 36, 383-408, https://doi.org/10.1007/s00603-002-0035-z, 2003.

Chen, H. K. and Tang, H. M.: Stability analysis method of perilous rock in source of avalanche, J. Geol. Min. Res., 2, 60-67, https://doi.org/10.5897/JGMR.9000070, 2010.

Chen, H. K., Xian, X. F., Tang, H. M., and Feng, Q. H.: A massive development mechanism and countermeasures for perilous rocks in the Three Gorges Reservoir area of PR China: The example of the Taibaiyan cliff at Wanzhou, Journal of Chongqing University, 31, 1178-1184, https://doi.org/10.11835/j.issn.1000-582X.2008.10.019, 2008.

Corominas, J., Mavrouli, O., and Ruiz-Carulla, R.: Magnitude and frequency relations: are there geological constraints to the rockfall size?, Landslides, 15, 829-845, https://doi.org/10.1007/s10346-017-0910-z, 2018.

Cruden, D. M. and Varnes, J. D.: Landslide types and processes. Landslides: investigation and mitigation, transportation research board (National Research Council), National Academy Press, Washington, DC, 1996.

D'Amato, J., Hantz, D., Guerin, A., Jaboyedoff, M., Baillet, L., and Mariscal, A.: Influence of meteorological factors on rockfall occurrence in a middle mountain limestone cliff, Nat. Hazards Earth Syst. Sci., 16, 719-735, https://doi.org/10.5194/nhess-16-719-2016, 2016.

Derron, M. H., Jaboyedoff, M., and Blikra, L. H.: Preliminary assessment of rockslide and rockfall hazards using a DEM (Oppstadhornet, Norway), Nat. Hazards Earth Syst. Sci., 5, 285-292, https://doi.org/10.5194/nhess-5-285-2005, 2005.

Ferrari, F., Giacomini, A., and Thoeni, K.: Qualitative Rockfall Hazard Assessment: A Comprehensive Review of Current Practices, Rock Mech. Rock Eng., 49, 2865-2922, https://doi.org/10.1007/s00603-016-0918-z, 2016.

Frattini, P., Crosta, G., Carrara, A., and Agliardi, F.: Assessment of rockfall susceptibility by integrating statistical and physically-based approaches, Geomorphology, 94, 419-437, https://doi.org/10.1016/j.geomorph.2006.10.037, 2008.

Frayssines, M. and Hantz, D.: Modelling and back-analysing failures in steep limestone cliffs, Int. J. Rock Mech. Min. Sci., 46, 1115-1123, https://doi.org/10.1016/j.ijrmms.2009.06.003, 2009.

Guzzetti, F., Reichenbach, P., and Wieczorek, G. F.: Rockfall hazard and risk assessment in the Yosemite Valley, California, USA, Nat. Hazards Earth Syst. Sci., 3, 491-503, https://doi.org/10.5194/nhess-3-491-2003, 2003.

Hutchinson, J. N.: Field and laboratory studies of a fall in Upper Chalk cliffs at Joss Bay, Isle of Thanet, in: Stress-Strain Behaviour of Soils, Proceedings of the Roscoe Memorial Symposium, Oxfordshire, 29-31 March 1971, 692-706, 1972.

Jaboyedoff, M., Baillifard, F., Philippossian, F., and Rouiller, J. D.: Assessing fracture occurrence using "weighted fracturing density": a step towards estimating rock instability hazard, Nat. Hazards Earth Syst. Sci., 4, 83-93, https://doi.org/10.5194/nhess-4-83-2004, 2004.

Jaboyedoff, M., Ben Hammouda, M., Derron, M.-H., Guérin, A., Hantz, D., and Noel, F.: The Rockfall Failure Hazard Assessment: Summary and New Advances, in: Understanding and Reducing Landslide Disaster Risk: Volume 1 Sendai Landslide Partnerships and Kyoto Landslide Commitment, edited by: Sassa, K., Mikoš, M., Sassa, S., Bobrowsky, P. T., Takara, K., and Dang, K., Springer International Publishing, Cham, 55-83, https://doi.org/10.1007/978-3-030-60196-6_3, 2021.

Kogure, T., Aoki, H., Maekado, A., Hirose, T., and Matsukura, Y.: Effect of the development of notches and tension cracks on instability of limestone coastal cliffs in the Ryukyus, Japan, Geomorphology, 80, 236-244, https://doi.org/10.1016/j.geomorph.2006.02.012, 2006.

Kromer, R., Lato, M., Hutchinson, D. J., Gauthier, D., and Edwards, T.: Managing rockfall risk through baseline monitoring of precursors using a terrestrial laser scanner, Can. Geotech. J., 54, 953-967, https://doi.org/10.1139/cgj-2016-0178, 2017.

Malamud, B. D., Turcotte, D. L., Guzzetti, F., and Reichenbach, P.: Landslide inventories and their statistical properties, Earth Surf. Process. Landf., 29, 687-711, https://doi.org/10.1002/esp.1064, 2004.

Matasci, B., Stock, G. M., Jaboyedoff, M., Carrea, D., Collins, B. D., Guerin, A., Matasci, G., and Ravanel, L.: Assessing rockfall susceptibility in steep and overhanging slopes using three-dimensional analysis of failure mechanisms, Landslides, 15, 859-878, https://doi.org/10.1007/s10346-017-0911-y, 2018.

Pérez-Rey, I., Muñiz-Menéndez, M., González, J., Vagnon, F., Walton, G., and Alejano, L. R.: Laboratory physical modelling of block toppling instability by means of tilt tests, Eng. Geol., 282, 105994, https://doi.org/10.1016/j.enggeo.2021.105994, 2021.

Pierson, L. A., Davis, S. A., and Van Vickle, R.: Rockfall hazard rating system–implementation manual, Federal Highway Administration (FHWA), Report FHWA—OR-EG-90-01, FHWA, US Department of Transportation, 80 pp., 1990.

Sagaseta, C.: On the Modes of Instability of a Rigid Block on an Inclined Plane, Rock Mech. Rock Eng., 19, 261-266, https://doi.org/10.1007/Bf01039998, 1986.

Santi, P. M., Russell, C. P., Higgins, J. D., and Spriet, J. I.: Modification and statistical analysis of the Colorado Rockfall Hazard Rating System, Eng. Geol., 104, 55-65, https://doi.org/10.1016/j.enggeo.2008.08.009, 2009.

Tang, H. M., Wang, L. F., Chen, H. K., and Xian, X. F.: Collapse sequence of perilous rock on cliffs with soft foundation, Chinese Journal of Geotechnical Engineering, 32, 205-210, 2010.

Volkwein, A., Schellenberg, K., Labiouse, V., Agliardi, F., Berger, F., Bourrier, F., Dorren, L. K. A., Gerber, W., and Jaboyedoff, M.: Rockfall characterisation and structural protection – a review, Nat. Hazards Earth Syst. Sci., 11, 2617-2651, https://doi.org/10.5194/nhess-11-2617-2011, 2011.

Ward, D. J., Berlin, M. M., and Anderson, R. S.: Sediment dynamics below retreating cliffs, Earth Surf. Process. Landf., 36, 1023-1043, https://doi.org/10.1002/esp.2129, 2011.

Wu, L. Z., Zhang, L. M., Zhou, Y., Xu, Q., Yu, B., Liu, G. G., and Bai, L. Y.: Theoretical analysis and model test for rainfall-induced shallow landslides in the red-bed area of Sichuan, Bull. Eng. Geol. Environ., 77, 1343-1353, https://doi.org/10.1007/s10064-017-1126-0, 2018.

Yu, B., Ma, E., Cai, J., Xu, Q., Li, W., and Zheng, G.: A prediction model for rock planar slides with large displacement triggered by heavy rainfall in the Red bed area, Southwest, China, Landslides, 18, 773-783, https://doi.org/10.1007/s10346-020-01528-x, 2021.

Zhan, J., Yu, Z., Lv, Y., Peng, J., Song, S., and Yao, Z.: Rockfall Hazard Assessment in the Taihang Grand Canyon Scenic Area Integrating Regional-Scale Identification of Potential Rockfall Sources, Remote Sens., 14, 3021, https://doi.org/10.3390/rs14133021, 2022.

Zhang, K., Tan, P., Ma, G. W., and Cao, P.: Modeling of the progressive failure of an overhang slope subject to differential weathering in Three Gorges Reservoir, China, Landslides, 13, 1303-1313, https://doi.org/10.1007/s10346-015-0672-4, 2016.

Zhang, M., Yin, Y. P., and Huang, B. L.: Mechanisms of rainfall-induced landslides in gently inclined red beds in the eastern Sichuan Basin, SW China, Landslides, 12, 973-983, https://doi.org/10.1007/s10346-015-0611-4, 2015.

Zheng, L. N., Chen, J. B., Zhou, Q. J., Feng, S. Q., Luo, Y. B., and Shen, P.: Experimental study on bearing capacity of moderately weathered mudstone in Chengdu area, Chinese Journal of Geotechnical Engineering, 43, 926-932, https://doi.org/10.11779/CJGE202105017, 2021.

Zhou, C., Yin, K. L., Cao, Y., Ahmed, B., Li, Y. Y., Catani, F., and Pourghasemi, H. R.: Landslide susceptibility modeling applying machine learning methods: A case study from Longju in the Three Gorges Reservoir area, China, Comput. Geosci., 112, 23-37, https://doi.org/10.1016/j.cageo.2017.11.019, 2018.

Zhou, Y., Shi, S., Zhang, Y., Cai, Q., Liang, J., and Cheng, Y.: Stability of unstable rock in nearly-horizontal sandstone-mudstone stratum due to enlarged rock-cell, Journal of Engineering Geology, 25, 1220-1229, https://doi.org/10.13544/j.cnki.jeg.2017.05.006, 2017.